E. Paz, Y. Ballesteros, F. Forriol Campos, N. Dunne, J.C. del Real-Romero, **Graphene and graphene oxide functionalisation with silanes for advanced dispersion and reinforcement of PMMA-based bone cements**. *Materials Science & Engineering C-Materials for Biological Applications*. Vol. 104, pp. 109946-1 - 109946-12, Noviembre 2019. [Online: Julio 2019]

https://doi.org/10.1016/j.msec.2019.109946

Graphene and Graphene Oxide Functionalisation with Silanes for Advanced Dispersion and Reinforcement of PMMA-based Bone Cements

E. Paz*[(1)], Y. Ballesteros[(1)], F. Forriol[(2)], N.J. Dunne[**(3-6)], J.C. del Real[**(1)]

(1) Institute for Research in Technology /Mechanical Engineering Dept., Universidad Pontificia Comillas, Alberto Aguilera 25, 28015, Madrid, Spain

(2) School of Medicine, Universidad San Pablo CEU, Urb. Monteprincipe, 28925 Alcorcon, Madrid, Spain

(3) Centre for Medical Engineering Research, School of Mechanical and Manufacturing Engineering, Dublin City University, Stokes Building, Collins Avenue, Dublin 9, Ireland

(4) School of Mechanical and Manufacturing Engineering, Dublin City University, Stokes Building, Collins Avenue, Dublin 9, Ireland

(5) School of Pharmacy, Queen's University Belfast, 97 Lisburn Road, Belfast BT9 7BL, United Kingdom

(6) Trinity Centre for Bioengineering, Trinity Biomedical Sciences Institute, Trinity College Dublin, Dublin 2, Ireland

Highlights: Bone cement, Graphene, Functionalisation, Silane, Reinforcement

* Corresponding author:
Dr Eva Paz Jiménez
Email: eva.paz@comillas.edu

** Joint last authors:
Professor Nicholas J. Dunne
Email: nicholas.dunne@dcu.ie

Dr Juan C. del Real
Email: delreal@comillas.edu

Abstract

The reinforcement of PMMA bone cements using carbon based nanomaterials has demonstrated to be a potential solution to their poor mechanical properties. The achievement of an optimal dispersion of the nanoparticles within the polymeric matrix is a crucial but not easy stage in the production of high-quality reinforced materials. In this work, an useful route for the **graphene** (G) functionalisation, via silanisation with **3-methacryloxypropyl)trimethoxy silane** (MPS), has been developed, providing a remarkable enhancement in dispersability and mechanical properties. With the purpose to define the critical graphene surface oxidation parameters for an optimal silanisation, different routes were thoroughly analysed **using infrared spectroscopy (FTIR), thermogravimetric analysis (TGA), X-ray photoelectron spectroscopy (XPS) and scanning electron microscopy (SEM).** The results showed that the silanisation significantly improved the G dispersability: whereas the pristine G dispersion fell down within the first 24 h, the silanised G showed an adequate stability after 5 days. Additionally, this improved dispersability produced a notable increase in the mechanical properties of the G-reinforced bone cements: in comparison with the pristine G, the compression and bending strength of silanised G increased by 12% and by 13.7% respectively **and the fracture toughness by 28%.** These results provide very useful information on the relevance that the characteristics of the superficial oxidation of graphene have on the effectiveness of the silanisation process, besides an interesting functionalisation procedure for advanced dispersion and reinforcement of G-PMMA bone cements.

Graphical Abstract

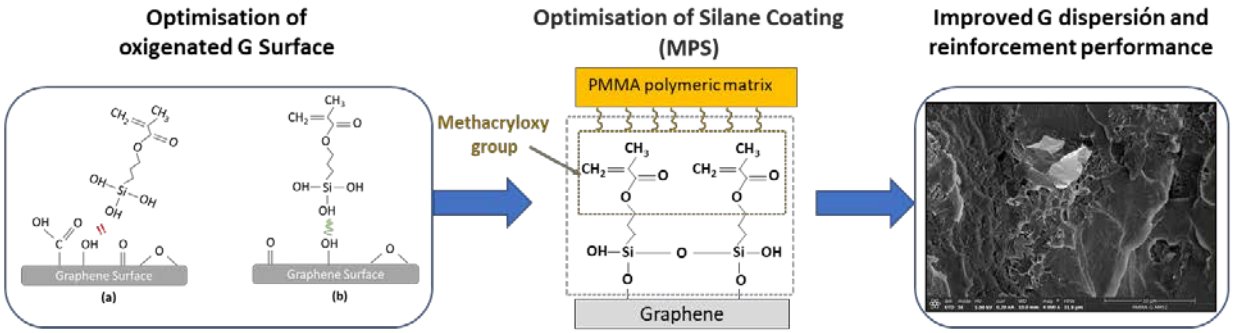

1. Introduction

Recently, carbon based nanomaterials (CBN) have been shown to be an interesting solution in the reinforcement of polymer composites [1-6] with different purposes and applications. Some of these applications are directed towards electromagnetic interference shielding [7,8], electrically conductive nanocomposites [9], energy storage and conversion [10,11], catalysis [12,13], environmental solutions and mechanical reinforcement among others [14,15].. The incorporation of various types of CBN, including carbon nanotubes (CNT), graphene (G), graphene oxide (GO), carbon fibers or carbon black, into different polymeric matrix have enhanced the mechanical properties of the pristine polymer [16-22]. It has been postulated that a good dispersion of CBN within the polymer matrix produces a deviation and detention of crack fronts during their propagation, increasing the required energy for failure [23,24]. In particular, this mechanism has a notable effect in the improvement of the fatigue life and fracture toughness of these nanocomposites.

Homogenous dispersion of the CBN throughout the polymer matrix has been shown to be crucial in the final performance of such composites since poor dispersion and deficient interaction between the CBN and the polymer matrix can produce weak zones and aggregates that favour crack propagation [16,18]. The aggregation or restacking of these nanomaterials, their poor dispersion and the weak interactions between them and the polymeric matrix are considered the most important limitations that weaken their great potential.

There have been explored many solutions, physical and chemical methods, to improve the dispersability during the preparation of these nanocomposites [25,26]. The functionalisation of CBN has been one of the most explored options to deal with the aforementioned limitations. The introduction of chemical functional molecules onto the surface of the CNB can help to bridge the nanoparticle and the polymer, improving nanoparticle dispersion and enhancing the chemical interlocking between nanoparticle and matrix [27]. Many types of functionalisation routes, through covalent and noncovalent bonds, have been investigated with varying degrees of success [28].

The reinforcement of PMMA based bone cements with CBN has been recently explored. These polymeric materials are primarily used as grouting agents in the support of the prosthesis within the bone during the joint replacement surgery [29,30]. Notwithstanding

the many advantages that PMMA based bone cements demonstrate, they do have some important drawbacks that can compromise the long-term success of joint replacement surgery, increase associated costs and consequently impact the patient's quality of life [30,31]. Aseptic loosening is considered to be one of the major causes of implant failure, which has been mainly ascribed to fracture or fatigue failure of the cement mantle that surrounds the implant [32]. Therefore, the reinforcement of these bone cements using different materials has been widely investigated [33]. Regarding the use of CBN, the incorporation of multi-walled carbon nanotube powders (MWCNT) and recently the use of G and GO, have demonstrated important enhancements in the static mechanical properties, fracture toughness and fatigue life of bone cements when an optimal CBN loading level was used [34-37]. Repeatable and reliable homogenous dispersion of the CBN in the bone cement matrix has been reported to be the one most complicated issue to address, with ultrasonication of the CBN in the liquid phase being cited as the optimal method for effective dispersion. Additionally, Ormsby et al. [34] demonstrated that a good strategy to improve MWCNT dispersion was through the use of carboxyl functionalised MWCNT (4 wt.% COOH) as opposed to its unfunctionalised counterparts.

In the preparation of other types of polymer nanocomposites, the silanisation of CBN has been presented as a very interesting alternative [38,39,40]. Silane coupling agents are compounds whose molecules contain functional groups that bond with both organic and inorganic materials. A silane coupling agent acts as a sort of intermediary, which promotes adhesion between organic materials to inorganic materials [41]. The typical structure of these molecules is: $(RO)_3SiCH_2CH_2CH_2$-X, where (RO) is a hydrolysable group (e.g. methoxy, ethoxy, or acetoxy, and X is an organofunctional group, such amino, methacryloxy, epoxy). The silanisation of several nanosized reinforcements, as different kind of nanofibers or nanoparticles, has demonstrated substantial improvements in their dispersion and interface bonding with the matrix. In the case of carbon nanotube powders (CNT) in the first instance, and subsequently of G and GO, these demonstrated interesting results in the reinforcement of polymeric composites (e.g. epoxy composites) [6,16,42,43]. These types of carbonaceous surfaces usually required prior oxidation of their surface in order to introduce oxygenated groups for the reaction and anchorage of the silane molecules. A plethora of silane coupling agents have been investigated, which include: (3-methacryloxypropyl)trimethoxy silane (MPS), (3-aminopropyl)triethoxy silane (APTES), (3-aminopropyl)trimethoxy silane (APTMS), (3-

glycidyloxypropyl)trimethoxy silano (GPTMS) or triethoxymethylsilane (MTES) with varying degrees of success reported [44-46]. It has been observed that the effectiveness of the CBN silanisation depends on several factors: (1) compatibility of the organosilane with the polymeric matrix and CBN surface, or (2) the silanisation route and associated parameters used (e.g. silane concentration, hydrolysis and silanisation times, temperature and pH) [42,43,47,48].

The many studies conducted to date have demonstrated the advantages of silanes for numerous applications [38-40,45-52]. Many of these research studies focused on the optimisation of the silanisation procedure, demonstrating the final performance of these coupling agents are highly dependent on different silanisation parameters [49,50]. The effect of hydrolysis time [51], concentration of the silane solution [47] and the time and temperature during the condensation [52] are some of the parameters that have been extensively investigated. However, in the case of the CBN, often a previous oxidation step of the surface is required to promote anchoring of the silane molecules (Figure 1), no studies have been reported on the effect that the oxidation features have on the silanisation performance. Taken in consideration the notable effect that other parameters have on the silane effectiveness, the proposed novelty of this research study is the analysis of the relationship between the surface oxidation features and the silanisation performance, with the objective of enhancing the reinforcement potential of CBN in the preparation of nanocomposites. This study aims to design, optimise and validate a specific functionalisation procedure using a silane coupling agent that potentiates G as a reinforcing agent in PMMA-based bone cement.

The designed silanisation route used 3-methacryloxypropyltrimethoxysilane (MPS), this was chosen as the methacryloxy groups present in MPS has the potential to exhibit good compatibility with the methyl methacrylate (MMA) within the bone cement and consequently favour strong interaction and promote adhesion between the G or GO powder and the PMMA bone cement (Figure 1).

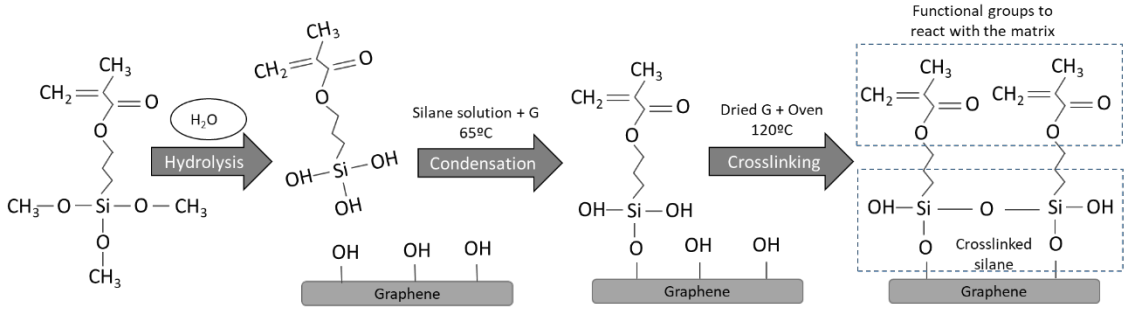

Figure 1: Schematic representation of the silane molecules reactions with the graphene surface.

To gain a better understanding of the silanisation mechanism, it has been analysed how the oxidation route influences the type and degree of oxidation achieved on the G surface. Thus, the effect of these parameters with respect to silanisation efficiency and therefore in the extent of reinforcement has been determined. For this purpose, a similar silanisation procedure was applied following different oxidation routes. The resultant G and GO powders produced from silanisation were characterised using Fourier transform infrared spectroscopy (FTIR), X-ray photoelectron spectroscopy (XPS), thermogravimetric analysis (TGA), the morphological changes of the nanoparticles and its dispersion were also evaluated using scanning electron microscopy (SEM). Finally, the different G and GO powders were incorporated into PMMA based bone cement and the static mechanical properties as per ISO 5833: 2002 were also studied [53]

The results of this research demonstrate that the surface oxidation features are very important parameters for the optimisation of silanisation routes. It suggests that it is more important the type of oxygenated group (preferable hydroxyl groups), than the degree of surface oxidation; being possible that a high presence of other type of oxygenated groups (e.g. carboxyl groups) impair the formation of a high-quality silane coating on the G surface.

2. Materials and methods

2.1. Materials

2.1.1. Bone cement

The bone cement used was a two-part acrylic based system [22,23] (Table 1). The powder phase was mainly composed of Colacryl B866 (Lucite International Ltd., UK), it is a pre-polymerised PMMA powder that was supplied pre-blended with the initiator (benzoyl peroxide, BPO). Barium sulphate was the radiopaque agent (Sigma Aldrich, UK) and was subsequently added to the powder component. The liquid phase was composed of the monomer (methyl methacrylate, MMA) the activator of polymerisation (N,N-Dimethyl-p-toluidine, DmpT) and hydroquinone (all supplied by Sigma Aldrich, UK). The bone cement formulation described was analogous to the commercial bone cement, DePuy CMW[1] [22].

Table 1: Composition of the PMMA based bone cement.

Powder phase		
Pre-polymerised polymer	Colacryl 866 - Polymethyl methacrylate (PMMA)	36.36 g
Initiator	Colacryl 866 - Benzoyl peroxide (BPO)	
Radiopaque Agent	Barium Sulphate ($BaSO_4$)	3.64 g
Liquid phase		
Monomer	Methyl methacrylate (MMA)	19.9 mL
Activator	N,N-Dimethyl-p-toluidine (DmpT)	160 mL

2.1.2. Nanomaterials

In this study, powders of graphene (G) (Avanzare Nanotechnology, Spain) and graphene oxide (GO) (NanoInnova Technologies, Spain) were added to the acrylic bone cement. According the supplier data sheets, the G powder is composed of 1 - 2 layers of graphene sheets with an average lateral size of 50 – 500 nm and a thickness of 0.7 nm; the GO sheets have an average lateral size of 1.8 – 2.7 nm and a thickness of 0.7 – 1.2 nm.

2.1.3. Silane coupling agent and reagents

A silane coupling agent, 3-methacryloxypropyltrimethoxysilane (MPS) (ABCR Gmbh, Germany), was used during the functionalisation of G and GO. The silane was selected based on the hypothesis the methacryloxy functional group would be the most appropriate to improve the compatibility with the MMA of the PMMA bone cement [55]. Other reagents were also used – i.e. ethanol 96% was used during silane hydrolysis of the silane.

Nitric acid 65%, hydrogen peroxide 30 % w/v and sulphuric acid 96% were used during the different G oxidation procedures. All were supplied by PanReac AppliChem (Spain).

2.2. Experimental procedure

2.2.1. Bone cement preparation

For the PMMA bone cement containing G or GO powder - 0.1 wt.% of G or GO was dispersed in the liquid monomer of the bone cement using ultrasonication (Digital Sonifier 450, Branson Ultrasonics Corporation, USA) at 50% amplitude for 3 min. To prevent overheating, the liquid monomer was placed in a waterbath that was held at 22 ± 1 ^{o}C. Each ultrasonication stage comprised of 30 s period followed by dwell of 10 s. Following sonication the suspension was placed in an ultrasonic bath (elmasonic p60h, Elma Schmidbauer GmbH, Germany) for 1 min - to reduce the incidence of bubble formation. PMMA bone cement without G or GO powder was used as the control cement for comparative purposes.

The bone cement was prepared under ambient conditions (22 ± 1 ^{o}C) and at a relative humidity of not less than 40% using the HiVac® Vacuum Mixing System (Summit Medical, Gloucestershire, UK) under a reduced pressure of 70.0±0.1 kPa, as per the manufacturer's instructions.

All tests specimens were fabricated using PTFE moulds. The bone cement was injected into each PTFE mould at 45 ± 1 s, the mould was then closed and the bone cement was allowed to cure for a minimum of 24 ± 0.5 h. Subsequently, each bone cement specimen was removed and the roughened edges were removed using 1200 µm grit silicon carbide abrasive. Test specimens were then stored at 22 ± 1 ^{o}C and at a relative humidity of not less than 40%for 1 week before testing. A total of three batches were prepared for each cement combination and at least five specimens were produced from each mix each one for each test type.

2.2.2. Nanomaterials functionalisation

The chemical functionalisation of the nanomaterials was performed in two steps in the case of the G (oxidation and silanisation) powder and only in one step for the GO (silanisation) powder. **The used oxidation and silanisation routes are based on the developed routes by other authors, this literature has been used as a starting point and some modifications have been completed to optimise the procedure [29,30,39].**

Prior to silanisation, it was necessary to oxygenate the G as anchoring of the silane molecules to the surface occurs via reaction with oxygenate groups. In order to evaluate the effect that oxidation has on the silanisation process - two different oxidation procedures were adopted which resulted in the production of two different versions of silanised G. With respect to the first oxidation procedure, step one involved adding 0.3 g of G into 70 mL of nitric acid (HNO_3) at 3 mole concentration. The solution was held at 60 ºC and magnetically stirred at 800 rpm for 15 min. Thereafter, 20 mL of suspension was placed a covered glass tube, which was placed in an ultrasonic bath (elmasonic p60h, Elma Schmidbauer GmbH, Germany) for 1.5 h at 37 Hz and 100 W; then the G powder was filtrated and washed using deionised water. For step two – the resultant G powder was treated following the process outlined in step 1 – with the exception that 70 mL of hydrogen peroxide (H_2O_2) (30% w/v) was used instead of HNO_3. Finally, the obtained G powder after the two-step process (*G_Oxi1*) was freeze dried overnight using a Telstar LyoQuest freeze dryer (Telstar, The Netherlands). The second oxidation procedure was developed as a single-step process - 0.5g of G powder were added to 100 mL of a solution (75:25 v/v) of H_2SO_4 (96%):NHO_3 (3M). The suspension was held at 60 ºC and magnetically stirred for 15 min at 800 rpm, thereafter it was placed into 20 mL glass tubes that were covered and then placed into the ultrasonic bath for 2 h at 37 Hz and 100 W. Finally, the resultant G powder was washed, filtrated and freeze dried; the obtained product was termed *G_Oxi2*.

In relation to the silanisation process, the first step is the hydrolysis of the silane molecules, for this a 100 mL solution of ethanol:deionised water (80:20 v/v) was prepared and the pH was adjusted to 3.5-4.5, then the same mass of MPS to the mass of nanoparticle to be silanised was added to the solution and then magnetically stirred for 30 min at 800 rpm under ambient conditions. Thereafter, the G_Oxi1, G_Oxi2 or GO were added to the solution and initially dispersed using ultrasonication for 10 min, and then magnetically

stirred for 2 h at 800 rpm at a temperature of 65 ºC. Once the liquid was evaporated, the residual powder was washed and freeze dried**. The dried powder was then placed into an oven held at 120 ºC for 2 h to favour the crosslinking of the silane molecules.** The resultant graphene powder was termed *G_MPS1*, *G_MPS2* and *GO_MPS*.

2.2.3. Nanoparticle characterisation

The FTIR spectra of the powder based nanomaterials were recorded using a Bruker Tensor 27 spectrophotometer (Bruker Española S.A, Spain) in the spectral range of 4000-600 cm^{-1}. Specifically, discs of 300 mg of KBr with 0.5-1 mg of powder nanomaterial were prepared using an arrangement and a press specifically designed by the spectrophotometer manufacturer. The obtained spectra were processed and evaluated using the OPUS software (Bruker Optics, Germany).

Thermogravimetric analysis (TGA) was conducted to obtain further information relating to the degree of functionalisation and thermal stability as a function of using the oxidation and silanisation procedures. The samples (5-10 mg) were placed in platinum pans and characterised using a Stanton Redcroft DTA/TGA 1600 (Rheometric Scientific, UK) using a heating rate of 20 ºC/min from 0 to 700 ºC. Each test was performed in triplicate and the data analysed using the RSI Orchestrator software (Rheometrics Scientific, UK).

X-ray photoelectron spectroscopy (XPS) analysis was conducted to determine the elemental composition of the graphene powders. It was performed using a V.G. Scientific Microtech Multilab spectrometer (VG Microtech, UK) with a Mg Kα achromatic X-ray source (1253.6eV) operating at 50keV pass energy and 300 W. The pressure inside the analysis chamber was maintained below 500 Pa during analysis and measurements were taken using a take-off angle of 45º. Survey scans were taken in the range 0-1100 eV and high resolution scans were obtained for all significant peaks in the survey spectra. Binding energies for all photopeaks were referenced to the C1s photopeak position for C-C and C-H species at 284.6 eV. Multi-component carbon 1s photopeaks were curve fitted using photopeaks of Gaussian-Lorentzian (70-30%) peak shape with a full-width-at-half maximum (FWHM) of 1.8±0.1 eV.

Scanning Electron Microscopy (SEM) was used to analyse the size and morphology of the different graphene powder using a XL-30 Scanning Electron Microscope (Philips, The Netherlands). The energy of the electron beam was 10 kV. The nanoparticles were

dispersed in MMA and deposited in a sample carrier, thereafter the MMA was evaporated and the deposited nanoparticles were coated with gold, providing a conducting medium for the electrons and sufficient contrast for the SEM images.

2.2.4. Evaluation of the dispersion

In order to evaluate the stability of the graphene powder based suspensions in MMA, suspensions of 0.005 mg of powder in 10 mL of MMA were prepared using ultrasonication with a Digital Sonifier 450 (Branson Ultrasonics Corporation, USA). Specifically, each sample was sonicated for 3 min (30 sec ON and 10 sec OFF) at 50% amplitude.

Each suspension was placed in a transparent tube and natural sedimentation was observed as a function of time over a 120 h period (i.e. 0 h, 24 h, 48 h and 120 h).

2.2.5. Mechanical characterisation

The compression and bend properties were determined in accordance with ISO 5833 [53]. Compression tests were performed with cylindrical specimens of 12.0 ± 0.1 mm length and 6.0 ± 0.1 mm diameter using a Universal Testing Machine ELIB 20W (Ibertest, Spain) with a load cell of 20 kN. The machine operated at a crosshead speed of 20 mm/min until specimen failure. The compressive strength was subsequently calculated from the load versus deformation data, dividing the maximum force by the original cross-sectional area [53]. A four-point bending load arrangement was used to determine the bend properties. Specimens were in the form of rectangular bars with dimensions of 80.0 ± 0.1 mm length, 10.0 ± 0.1 mm width and 4.0 ± 0.1 mm thickness. The tests were conducted using a Universal Testing Machine IBTH/500 (Ibertest, Spain) using a load cell of 5 kN, operating at a crosshead speed of 5 mm/min. The bend strength (σ) and bend modulus (E) was calculated as per ISO 5833 [53]. For measurement of the compression and bend properties – a total of three batches were tested for each cement composition with a minimum of five samples per batch.

The fracture toughness was determined according to the standard [54]. Single edge notch bend specimens (SENB) were used to calculate the fracture toughness. The tests were performed under three-point bending loading arrangement using a Universal Testing Machine IBTH/500 (Ibertest, Spain); the cross-head rate was 0.5 mm/min. Rectangular specimens of 61.6 ± 0.1 x 14.0 ± 0.1x 7.0 ± 0.1 mm were used.

Prior to the testing, a notch was machined in each specimen and a pre-crack was generated according the standard specification outlined in ASTM D 5045 [54].

2.3. Statistical Analysis

The mean values of the results were evaluated for statistical significance using a one-way analysis of variance (ANOVA) test with a post-hoc Scheffe´s test (SPSS 15.0 for Windows; IBM SPSS, USA). A p-value less than 0.05 was indicative of statistical significance.

3. Results & Discussion

3.1. Nanoparticle characterisation

3.1.1. Fourier Transform Infrared Spectroscopy analysis

The characteristic vibration of the C=C at 1633 cm^{-1} was observed from the spectrum for G (Figure 2 (a)), which was attributed to the aromatic carbon structure of G, GO and carbon nanotubes [45,56-58]. The remainder of the peaks may be attributed to some degree of oxidation of the pristine G in addition to the atmospheric moisture. The band at 3450 cm^{-1} was be attributed to the adsorbed water and/or hydroxyl functional groups in the G surface [48,57,59], the peak at 1055 cm^{-1} corresponded with the C-OH vibrations of the alcohols [47,59] and the peaks at 1406 cm^{-1} and 1710 cm^{-1} was indicative of the presence of carboxyl groups [59,60]. In comparison with the pristine G spectrum, for the G_Oxi1 and G_Oxi2 spectra (Figure 2(b) and Figure 2(c)) it was possible to observe the emergence of peaks attributed to the oxygenated groups, which demonstrated the success of the oxidation procedures. From the G_Oxi1 spectrum, the presence of carboxyl groups at 1768 cm^{-1} (C=O), hydroxyl groups at 3454 cm^{-1} (O-H) and epoxy groups at 1217 cm^{-1} (C-O-C) were observed. Analysis of the G_Oxi2 spectrum indicated a higher degree of oxidation when compared with the G_Oxi1 spectrum. Stronger absorption bands were evident at 1722 cm^{-1}, 1217 cm^{-1} and 1053 cm^{-1} indicating an important presence of carboxyl, epoxy and alcohol groups.

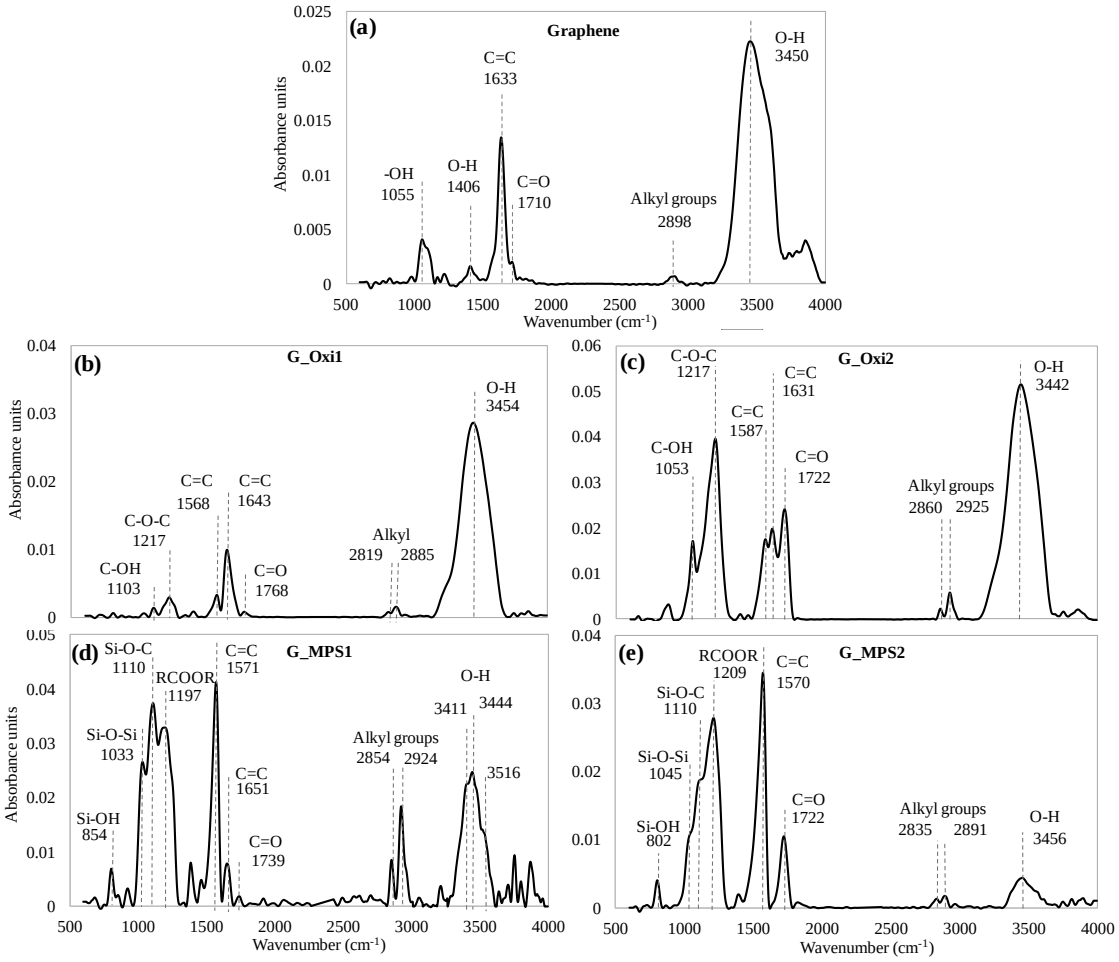

Figure 2: Fourier Transform Infrared Spectroscopy (FTIR) spectra of pristine graphene (A) and graphene powder following different methods of functionalisation: G_Oxi1 (B), G_Oxi2 (C), G_MPS1 (D) and G_MPS2 (E).

It is interesting to note the emergence of a band at 1568 cm^{-1} for the G_Oxi1 and at 1587 cm^{-1} for the G_Oxi2, this peak was assigned to the C=C stretching transitions of the graphitic domains following removal of the oxidative debris (OD) of the G powder. The OD is considered as an amorphous carbonaceous material with a high level of oxygen-content that is strongly adhered by non-covalent bonding to the G, GO or CNT surfaces [57]. Although the assignment of this peak is controversial, several authors have previously reported this shift of the C=C band due to the interaction of OD with G via π-stacking, affecting to the C=C stretching transitions [56,61,62]. The intensity of the peak corresponding to the C=C that appeared at 1587 cm^{-1} is higher in the case of G_Oxi2 when compared to G_Oxi1, indicating a greater level of OD removal, which corresponded to a higher degree of oxidation.

For the G_MPS1 spectrum (Figure 2 (d)) the peaks at 1033 cm^{-1} and 1110 cm^{-1} can be attributed to the Si-O-Si and Si-O-C bonds and confirmed the presence of silane groups

on the G surface post-silanisation [45,47,48,58,60,63]. These peaks also appeared in the G_MPS2 spectrum (Figure 2(e)) at 1045 cm^{-1} and 1110 cm^{-1}. The presence of the Si-O-C band corroborated that the silanisation was achieved via covalent bonds with the G surface and the presence of the siloxane groups (Si-O-Si) was indicative of the crosslinked level between the silane molecules during condensation. Silanol groups (Si-OH) can be observed in both spectra at 850 cm^{-1} (G_MPS1) and at 802 cm^{-1} (G_MPS2) [47,57,60]. The increase of the two bands in the range of 2820-2930 cm^{-1} post-silanisation was assigned to the stretching of symmetric/asymmetric methylene groups of the alkylsilane terminus [44,47,59,64], this band increased significantly for the G_MPS1. The reduction of the bands in the range of 3400-3500 cm^{-1} could correspond to the reaction of the hydroxyl groups with the silane molecules.

In order to compare the silanised spectra, these were normalised with respect to the band at 1570 cm^{-1} (corresponding with the C=C). The normalised spectra suggested a higher silanisation degree for the G_MPS1 when compared with the G_MPS2. This higher silanisation degree was observed due to the greater intensity of the Si-O-C peak for the G_MPS1 spectrum, a higher intensity of the bands assigned to the alkylsilane groups and a greater decrease of the band assigned to the hydroxyl groups. In addition, the relationship between the intensity of the peaks of Si-O-C and Si-O-Si ($I_{Si\text{-}O\text{-}Si}/I_{Si\text{-}O\text{-}C}$) can provide an indication of the degree of crosslinking of the silane coating (condensate silane per amount of surface bonded silane). The spectrum of the G_MPS1 showed a $I_{Si\text{-}O\text{-}Si}/I_{Si\text{-}O\text{-}C}$ = 0.71, whereas the G_MPS2 spectrum demonstrated a $I_{Si\text{-}O\text{-}Si}/I_{Si\text{-}O\text{-}C}$ = 0.59, which suggested that the silane coating on the G surface exhibited a higher degree of crosslinking for the G_MPS1 when compared to the G_MPS2.

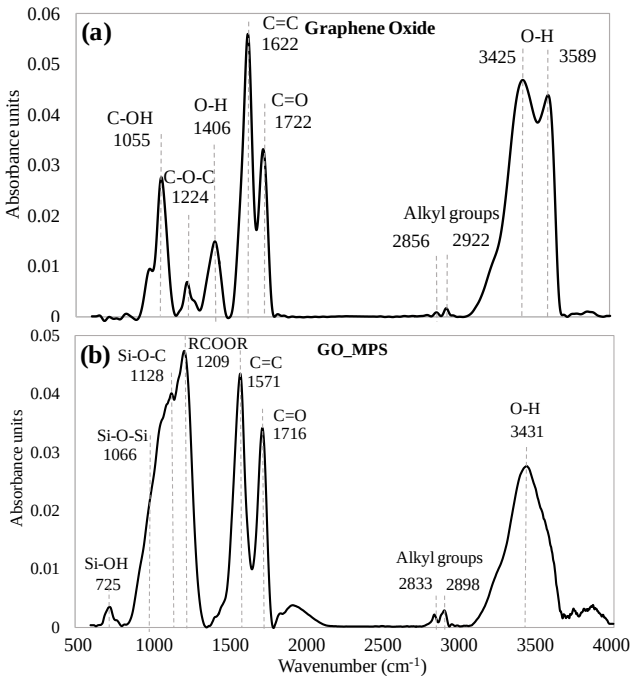

Figure 3: FTIR spectra of the pristine graphene oxide (A) and graphene oxide powder following silanisation: GO_MPS (B).

When the spectra of GO and the silanised GO (GO_MPS) were compared (Figure 3), the appearance of new bands at 725, 1066 and 1128 cm^{-1} in the GO_MPS spectrum suggests the formation of Si-OH, Si-O-Si and Si-O-C, which is indicative of the presence of silane on the GO_MPS surface. As well as in the silanised G, a decrease in the intensity of the -OH bands (3400-3600 cm^{-1}) and the shift of the peak assigned to C=C from 1622 cm^{-1} to 1571 cm^{-1} was also observed.

3.1.2. <u>X-ray photoelectron spectroscopy characterisation</u>

In order to analyse the surface chemical composition of the various G and GO powders (i.e. pristine, oxidised and silanised), X-ray photoelectron spectra (XPS) were used. Table 2 summarises the variation in the percentage of atoms of the different elements on the surface; the binding energy (BE) values for the C 1s, O 1s and Si 2p have been considered as 284, 531 and 102 eV [45,64]. Comparing the pristine G with the oxidised G - a significant increase in the oxygen concentration was observed, which was notably higher for the G_Oxi2 powder (21.41%) when compared to the G_Oxi1 (8.54%). This corroborated the FTIR data demonstrating the greater degree of oxidation observed for G_Oxi2. A small concentration of Si was detected on the surface of the oxidised G, since they had not been treated with the silane, which could be consequence of several factors (e.g. the reagent impurities & residues, post-production impurities on the graphene

surface and migration from the glass material). The silanised graphene also showed low Si content on their surfaces at levels of 0.71% and 0.31% for the G_MPS1 and G_MPS2. Although the level of Si detected is not significant, it is noticeable that there is an increase for the oxidised G when compared to the G_MPS1. These results support the higher degree of silanisation observed for the G_MPS1 from the FTIR data. The XPS also confirmed a decrease in the oxygen content after silanisation, which is possibly due a reaction between the oxygenated functional groups and the silane molecules. In the case of the silanisation of the GO powder a similar trend was observed, the Si content showed a moderate increase from 0.41% for the GO when compared to 0.47% for the GO_MPS. The oxygen content decreased from 33.30% for the GO powder to 20.27% for the GO_MPS, which was indicative of a reduction in the number of oxygenated groups. It is noticeable that the observed Si concentration is very small, but it is important to take into account that each silane molecule introduced into the structure contains only one atom of Si – but 10 atoms of C and five atoms of O.

Table 2: Concentration of atomic elemental species detected using XPS for pristine graphene, graphene oxide powder and their respective derivatives following different methods of functionalisation.

	C (%) (284 eV)	O (%) (531 eV)	Si (%) (102 eV)
G	95.44	4.48	0.08
G_Oxi1	91.07	8.54	0.39
G_Oxi2	78.29	21.41	0.29
G_MPS1	92.02	7.27	0.71
G_MPS2	85.75	13.94	0.31
GO	66.29	33.30	0.41
GO_MPS	79.25	20.27	0.47

3.1.3. Thermogravimetric analysis

Thermogravimetric analysis (TGA) was used to determine the efficiency of the G oxidation and silanisation and potential structural changes in the G and GO carbon structure as a function of the chemical treatments used. The TGA curves of G, G_Oxi1 and G_Oxi2 (Figure 4(a)) corroborated the high oxidation degree of G_Oxi2, with a greater weight loss before 550 ºC being attributed to the thermal degradation of the elevated amount of functional groups present on the surface [45,47,57,59,65,66]. A weight loss before 550 ºC was also observed for G_Oxi1, however this weight loss was significantly lower than when compared to G_Oxi2. It was also notable that the thermal

stability of the oxidised G showed a slight increase with respect the G, with a remaining weight of 14% at 700 ºC for the G_Oxi1 and of 13.5% for G_Oxi2, in comparison to 1.2% for the G powder.

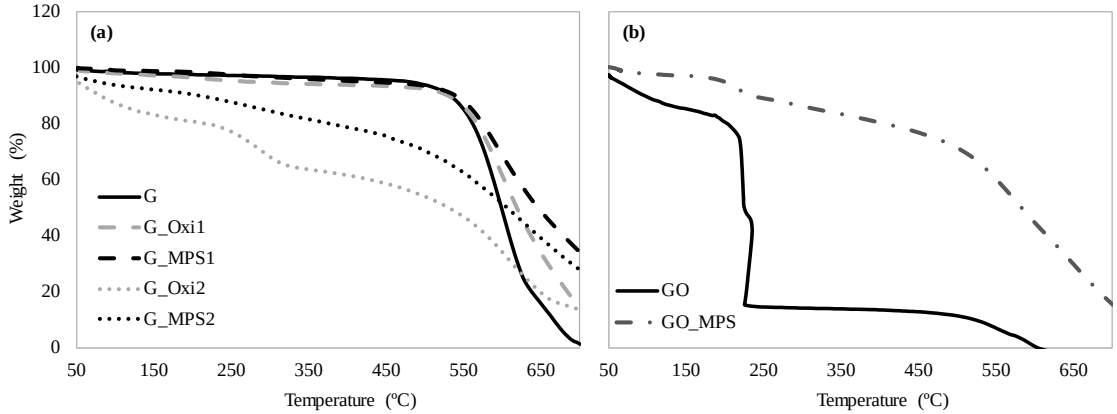

Figure 4: Weight loss curves obtained from TGA for pristine graphene (A), graphene oxide powder (B) and their respective derivatives following different methods of functionalisation.

In the case of the silanised G (Figure 4(a)) can be observed a remarkable increase in the thermal stability of G_MPS1 and G_MPS2 in comparison with the respectively oxidised G as well respect to the pristine G. The remainder weight at 700 ºC in the G_MPS1 was 34.0% and in the case of G_MPS2 was 27.7%. The higher thermal stability of G_MPS1 also could be considered as a higher silanisation degree [45].

The TGA curve for GO exhibited a low thermal stability with a sharp drop in the weight loss between 150-230 ºC due to the high level of oxygenated functional groups Figure 4(b). However, the thermal stability of the GO_MPS was largely enhanced following silanisation. The remaining weight for the GO_MPS at 700 ºC was 15.2%, while the GO was completely decomposed. A slight reduction for the GO_MPS curve between 150-230 ºC was also observed, which showed the presence of some oxygenated functional groups post-silanisation. These results are also in accordance with the FTIR spectra and XPS analysis.

3.1.4. <u>Morphological characterisation</u>

Scanning electron microscopy (SEM) was used to evaluate if the silanisation treatment produced any important changes in the morphological features of the G (**Figure 5)**. From the SEM images – no appreciable changes in the morphological features of the G powder (e.g. length, thickness or the formation of agglomerates) post-silanisation were observed.

Morphological features of the GO following dispersion were observed to be very different to the G nanoparticles.

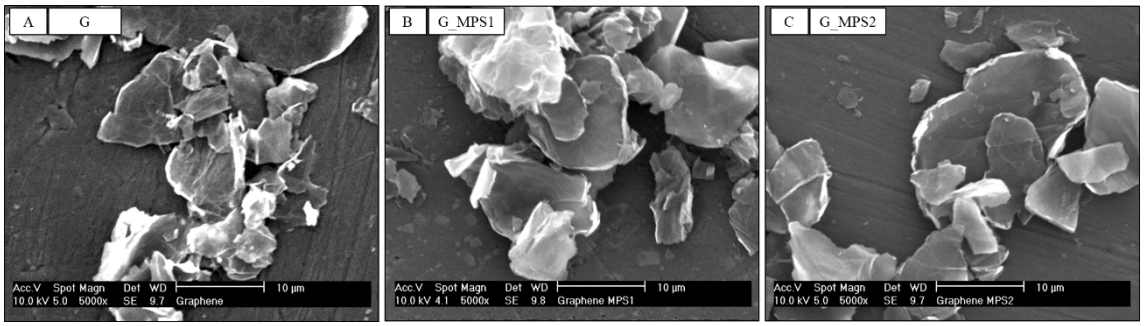

Figure 5: SEM images of G (G), G_MPS1 (B) and G_MPS2 (C) nanoparticles at 5000x magnifications.

The GO structure showed a less laminated morphology, forming a porous structure with the aspect of a “sponge”. Porous agglomerates of this structure were observed across a wide range of dimensions. However, post-silanisation, the GO morphological aspect showed important modifications, the particles or agglomerates exhibited a loss of porosity and a reduction of their dimensions. **Additionally, as can be observed in the images at different magnifications the GO nanoparticles dimensions showed poor homogeneity and a low aspect ratio.**

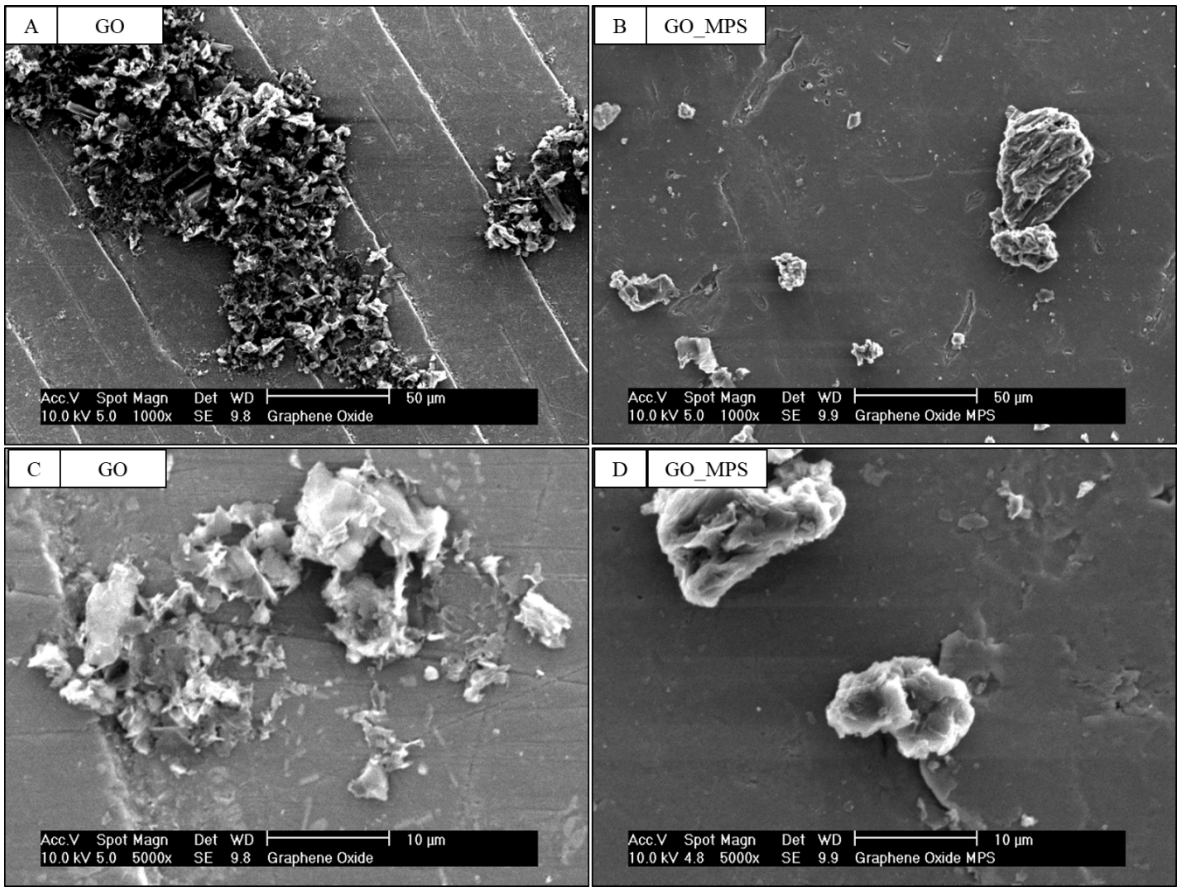

Figure 6: SEM images of GO and GO_MPS nanoparticles at 1000x (A, B) and 5000x magnification.

It is interesting to note the SEM images showed flakes of greater dimensions than those provided by the material supplier. It is suggested this could be attributed to the fact the materials supplier recorded dimensions of non-agglomerated GO. However, our SEM analysis demonstrated there is a wide variation in dimensions of the GO flakes (Figure 6).

3.2. <u>Evaluation of the dispersion</u>

Following sonication, a dark and homogeneous suspension with a similar aspect for the G, G-MPS1 and G-MPS2 was observed (**Figure 7**). However, the differences in the suspension stability between the G and the silanised G (G-MPS1 and G-MPS2) after 24 h were clearly evident: G suspension became clearer while the G-MPS1 and G-MPS2 suspensions remained dark and homogeneous. These differences become more pronounced as time progressed, it was possible to observe after five days, the G suspension was almost completely transparent, while a certain degree of nanoparticles within suspension remained in the G-MPS1 and G-MPS2. This means that the dispersion

stability was better for the G_MPS1 and G_MPS2 when compared to the G, indicating that the silanisation of the G improved its dispersion within the MMA monomer. Comparing the dispersion stability for the G-MPS1 and G-MPS2 suspensions, no important differences were detected.

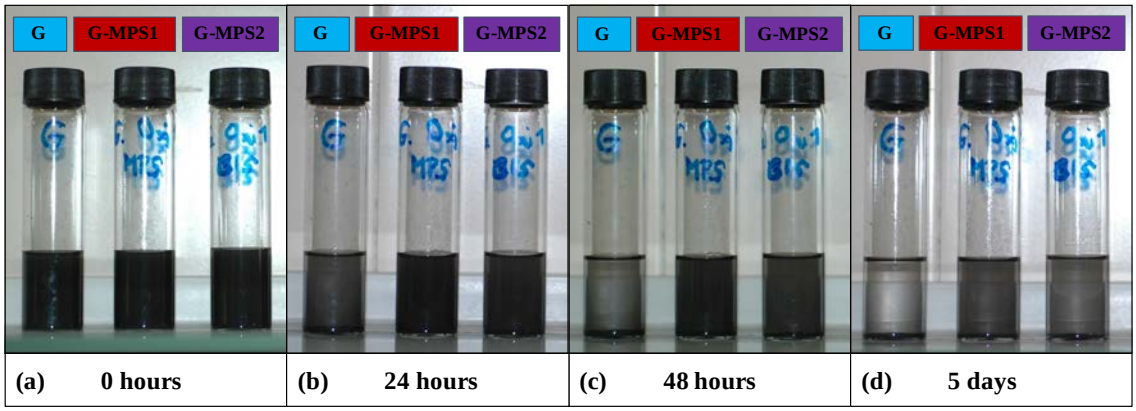

Figure 7: Evolution of the dispersion stability of G, G-MPS1 and G-MPS2 with the time: (A) 0 h, (B) 24 h, (C) 48 h and (D) 5 days following dispersion using sonication (concentration: $0.5 \cdot 10^{-3}$ mg/mL).

The GO and GO-MPS suspensions demonstrated different characteristics following sonication - the GO suspension was brown and the GO-MPS suspension was black (**Figure 8**). However, it is noteworthy that in both cases full sedimentation occurred within 24 h. The GO and GO-MPS suspensions became transparent earlier when compared to the G, G-MPS1 and GMPS2. In addition, no differences in dispersion stability were detected between the GO and the silanised GO, which implied the silanisation of the GO did not produce an improvement in dispersion stability within the MMA monomer.

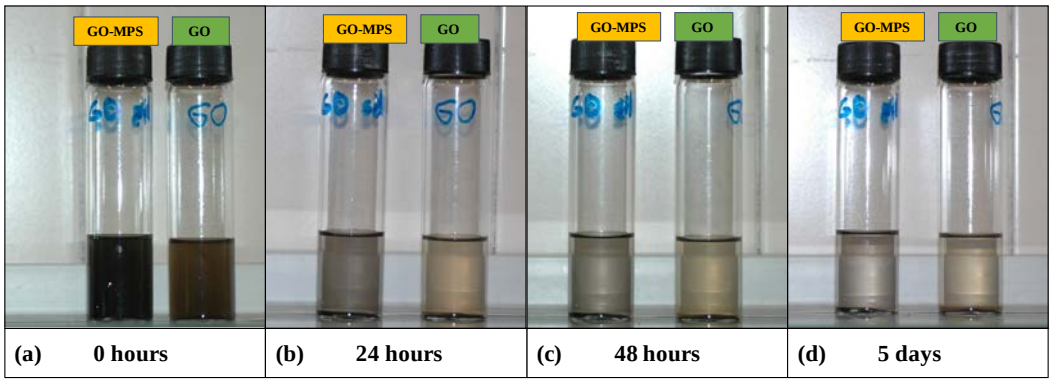

Figure 8: Evolution of the dispersion stability of GO and GO_MPS with the time: (A) 0 h, (B) 24 h, (C) 48 h and (D) 5 days following dispersion using sonication (concentration: 0.5·10-3 mg/mL).

Improved dispersion was also observed from the SEM analysis of the fracture surfaces of the specimens used in during mechanical testing. Some representative SEM images are shown in Figure 9. A high presence of G sheets agglomerates was observed in the case of the nanocomposite cements prepared using unfunctionalised G (Figure 9(a)). In contrast, the nanocomposite cements prepared with the silanised G demonstrated better dispersion of the G sheets within the cement matrix and no agglomerates were observed (Fig 9(b)).

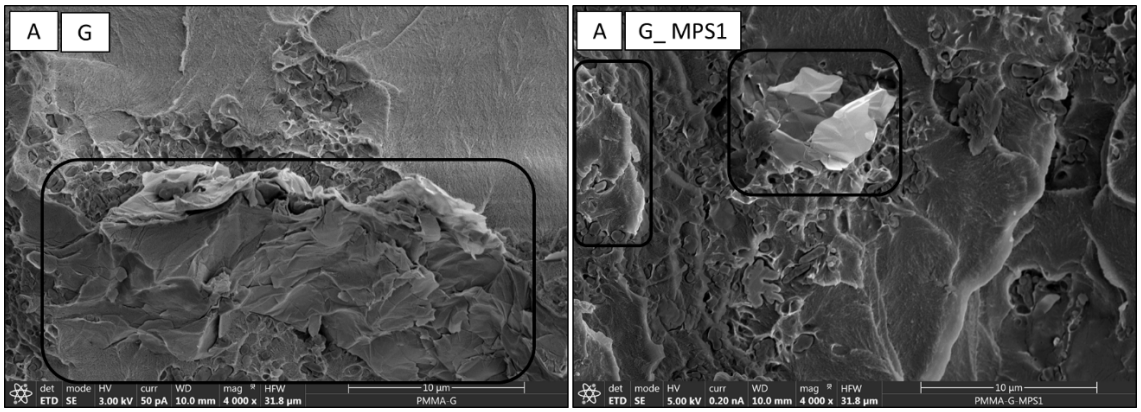

Figure 9: SEM images of fracture surfaces of bone cement with unfunctionalised G (A) and with G MPS1 (B) at 4000x magnification.

3.3. <u>Mechanical properties of bone cements</u>

As can be observed in Figure 10, bone cement containing G-MPS1 or G_MPS2 demonstrated a bending strength approximately 14.4% higher than similar cement containing pristine G and by approximately 16.7% when compared to the control cement. The improvement in the compression strength, as consequence of the silanisation, in comparison with the pristine G was approximately 12% (G_MPS1) and 10.3% (G_MPS2); whereas in comparison with the control was about 13.7% (G_MPS1) and 12.0% (G_MPS2). **Although these improvements are important, they did not show significant differences ($p<0.05$) when the mean values were statistically compared.**

In contrast to the mechanical data for the G powders, the silanisation of GO (GO_MPS) did not improve the mechanical properties of the resultant bone cements. Furthermore, the addition of GO_MPS reduced the bend strength of the bone cement by 10.6% when compared to the same bone cement containing GO powder.

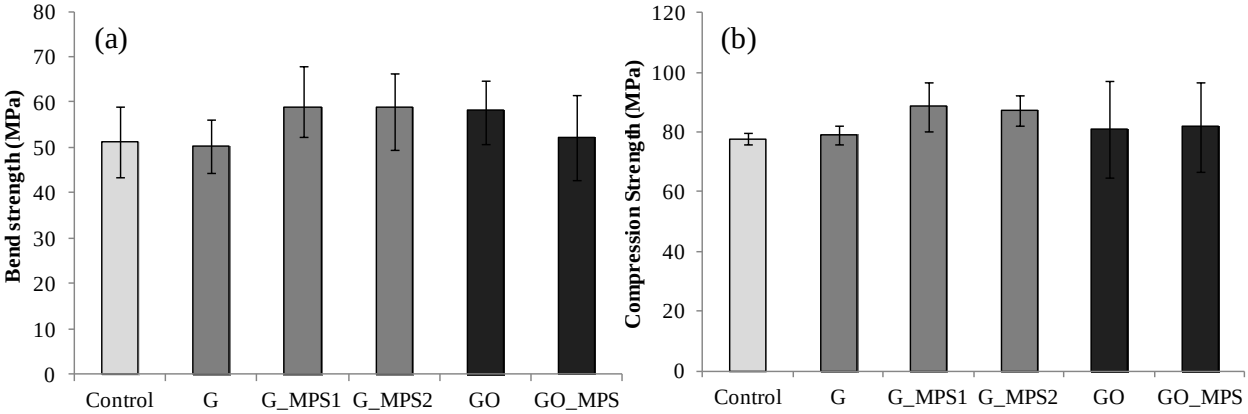

Figure 10: Mean bend strength (A) and compression strength (B) ± standard deviation (SD) of bone cements containing different G and GO powders, i.e. pristine form and following different methods of functionalisation & silanisation.

Table 3 shows the fracture toughness data for the different nanoparticles. Note the data for the silanised GO has been omitted due to low efficacy. However, the data for GO have been included to allow for comparison the silanised G.

Table 3: Fracture toughness (mean ± SD) for bone cements containing different G and GO powders, i.e. pristine form and following different methods of functionalisation & silanisation. It is considered significant differences between control and modified cement when p-value is less than 0.05.

	Fracture toughness ($MPa \cdot m^{1/2}$)	Variation vs control (%)	p-value vs Control
Control	1.30 ± 0.08	-	-
G	1.40 ± 0.07	7.6	0.2145
G_MPS1	1.67 ± 0.10	28.8	0.0128
G_MPS2	1.52 ± 0.06	17.2	0.2662
GO	1.53 ± 0.07	18.0	0.0391

Silanisation demonstrated greater improvements in fracture toughness when compared to the compression and bend strength. **The G_MPS1 increased the fracture toughness of the PMMA-based bone cement by approximately by 28% when compared to the control group ($p<0.05$); in comparison with the 7.7% of improvement achieved when the unfunctionalised G was incorporated ($p>0.05$). Additionally, although the differences were not significant when considering the compression and bend strength, the incorporation of G_MPS1 (1.67 ± 0.10 $MPa \cdot m^{1/2}$) to the PMMA-based bone cement exhibited notably higher levels of fracture toughness in comparison to GO (1.52 ± 0.07 $MPa \cdot m^{1/2}$).**

4. Discussion

This study demonstrated that the silanisation of G powder was a successful technique for enhancing its dispersion stability in MMA monomer and consequently the preparation of G-PMMA bone cements. In comparison with the pristine G, this improved dispersion produced an improvement in the bend, compression **and fracture** properties of the resultant bone cements. In contrast, the silanisation of the GO powder did not improve its dispersion in MMA monomer or demonstrate an increase in the mechanical properties of the resultant bone cement.

The efficacy of G and GO as reinforcement for PMMA bone cements has been reported in previous works, the optimal improvements were achieved when 0.1 wt% of G or GO were incorporated, being especially notable for the enhancement of the fatigue life and fracture toughness [37]. The results obtained in this work showed that the addition 0.1 wt% of G and GO in pristine form did not show significant improvements (**$p>0.05$**) in the bend and compression strength when compared to the control cement, but slight increments can be observed; these results are in accordance with the previously reported studies [37]. **In addition, the silanisation of the G using the proposed procedure 1 (i.e. G_MPS1) demonstrated a significant improvement ($p<0.05$) in the fracture toughness when compared with the unfunctionalised G.** The postulated mechanism by which the addition of G and GO powders to PMMA bone cement improved the static and fatigue properties is by the detention and deviation of the crack during its propagation, and this effect has greatest impact when considering fatigue and fracture failure [24,67]. However, such tests are complex and require considerable time to complete, therefore are not desirable when first approximations and evaluations are required. In this work it is remarkable that, in comparison with the pristine G, the silanisation of G produced an increase in the static mechanical properties **(i.e. compression, strength, bend strength and fracture toughness**) of 10-28% which can be considered a notable enhancement. However, in further work, once the silanisation method has been optimised, a thorough study of the mechanical behaviour in terms of the static and fatigue properties of bone cements containing silanised G should be completed.

The formation of aggregates and poor dispersion have been reported as the most common issues when considering CBN as a mode reinforcement for polymer based systems [6, 16,18]. The formation of aggregates and complications in obtaining a homogenous

dispersion of these nanoparticles have also been reported when incorporated into PMMA bone cements [37,68,69].

The silanisation of CBN has been demonstrated as an interesting alternative, improving the dispersion within different solvents and augmenting the mechanical properties of several polymer based composites a [46-48,60,64,70]. The optimal silanisation procedure should be tailored depending of several factors (e.g. the silane agent or the silanisation route); in most cases, this procedure is specific to a particular host polymer and nanoparticulate powder type.

Several studies have investigated how the silanisation mechanism works and how the different parameters influence its success (e.g. the amount of silane, the type of silane molecule or the route to link the silane agent onto the nanoparticle surface) [47,57]. However, there are few studies investigating how the type and degree of graphene oxidation, necessary to anchor the silane molecules on the surface [45,47,60], affects to the silanisation effectiveness.

The silanisation of G and GO and their incorporation into PMMA bone cements to date has not been investigated. It this work, additional to the development of an adequate silanisation route for the homogenous dispersion of G into the PMMA bone cement, it has been explored how the pre-oxidation of the G affects the linkage of the silane molecules to its surface.

It is postulated that the silanisation improves nanoparticle dispersion by acting as a coupling agent between the nanoparticles and the polymeric matrix - thereby promoting homogenous nanoparticle dispersion and adhesion to the polymer matrix. **A schematic of the silanisation process is represented in Figure 1. During the silanisation process the silane molecules are joined to the surface by the silanol groups (Si-OH). These silanol groups are firstly formed during the hydrolysis of the silane molecule. In a second step, the silanol groups reacts with the reactive groups introduced on the surface of the G nanoparticles via oxidation by the different routes proposed herein. In third step, once the silane molecules have anchored to the G surface, the crosslinking between the silane molecules is favoured by condensation at high temperature forming a coating over the surface, which causes the available functional groups (i.e. methacryloxy groups) to interact with the host polymer (with respect to PMMA bone cements, this is the MMA). Consequently, a high strength**

3D silane coating over the surface of the G nanoparticles is achieved via the crosslinking of the silane molecules, which promotes stronger bonding between the G nanoparticles and the MMA matrix of the PMMA bone cement.

In this work, two different routes of silanisation have been followed. The FTIR, XPS and TGA analysis demonstrated a higher silanisation in the G prepared by the procedure 1 (G_MPS1) than by the procedure 2 (G_MPS2). **This higher silanisation by the procedure 1 has resulted in improved fracture toughness for the PMMA-based bone cement (Table 3).**

A very interesting observation was that the G with the higher silanisation degree (G_MPS1) was obtained from the G with the lower oxidation level (G_Oxi1). This lower oxidation level for the G_Oxi1 was confirmed by FTIR, XPS and TGA analysis. Two aspects can be postulated as possible causes of this phenomenon, providing a better understanding about the silanisation mechanism:

(1) The type of oxygenate groups: The bonding of the silane molecules to the surface happens through the reaction between silanol and the oxygenated groups that are on the G surface [71,72]. In the silanisation reaction, among other parameters as the temperature or the pH, the properties of the surface prior to the silanisation process is a fundamental consideration [77-75]. It is believed that the interaction between the surface and the silane molecule happens through the reaction between the silanol groups present in the silane molecule and the hydroxyl groups on the substrate surface, which in this case is the previously oxidised graphene [71,76-79]. The results obtained in this study suggest that not all oxygenate groups have the same reactivity with the silanol groups. Therefore, oxidation that favours the formation of these hydroxyl groups on the surface will be a better option for the silanisation, being fundamental to the type of oxygenated groups present on the surface before the silanisation treatment.

This would explain why the G_Oxi2, having a higher content of oxygen, resulted in a lower degree of silanisation when compared to G_Oxi1. The FTIR analysis demonstrated that the content of carboxyl and epoxy groups in G_Oxi1 was negligible and the presence of hydroxyl groups was significant. In contrast, the FTIR spectrum of G_Oxi2 suggested a high content of carbonyl, epoxy and hydroxyl groups. However, post-silanisation, the peak with the highest reduction in intensity corresponded to the –OH.

Another interesting feature related to the differences between the oxidation procedures is the removal of oxidative debris, which could influence silanisation. The effect of the oxidative debris present on the graphene surface has been previously studied; demonstrating that the oxidative debris can significantly modify G properties (e.g. reactivity, conductivity or the dispersion stability) [56]. The results obtained in this work suggest that a low removal of the oxidative debris in the case of the G_Oxi1 could be beneficial for the silanisation. The oxidative debris has a high content of oxygenate groups and hydroxyl groups; although the oxidative debris is not covalently bonded to the G, the bonding of the silane molecules to G could be effective [56,61].

(2) The steric hindrance: Although a high presence of functional groups on the surface of the oxidised graphene may be advantageous, this present an obstacle during silanisation in two ways. Firstly, if the silanol prefers to react with the hydroxyl group, which are in close proximity to groups exhibiting less reactivity but at a higher volume, then these larger groups could make it difficult for the silanol to react with the hydroxyl groups due to steric hindrance [80,81]. Secondly, once the silane molecules are bonded onto the graphene surface, they need to be relatively close to facilitate condensation and crosslinking between them. If a higher number of other functional groups are present between the silane molecules, these functional groups could impair crosslinking due to steric hindrance or even through reaction with the silane reactive groups. This would explain the higher crosslinking and the higher degree of silanisation observed in the FTIR spectra for the G_MPS1 when compared with the G_MPS2. This higher crosslinking was potentially responsible of the higher thermal stability observed in the TGA data for the G_MPS1.

In further studies it will be interesting to investigate if the degree of silanisation has an effective influence in the mechanical performance of PMMA bone cement by investigating the fatigue properties. It would also be noteworthy, once the effect of oxidation is wholly understood, to optimise the silanisation process by studying the influence of different silane amounts and silanisation times in addition to other parameters.

On the contrary to the successful results obtained in the silanisation of the pristine G, the silanisation of the pristine GO did not produce improvements either in terms of its dispersion stability or mechanical properties of the resultant GO-PMMA bone cement.

However, the chemical analysis of the GO_MPS with the FTIR spectroscopy supported the presence of silanes, the XPS analysis indicated a decrease in the oxygenate groups and the TGA showed an improvement of the thermal stability of the GO post-silanisation. Using SEM, it is postulated that silanisation of the GO did not result in the augmentation of mechanical properties due to the morphology of the GO particles. **A high aspect ratio is a very important characteristic of the nanoparticles in order to promote reinforcement. However, SEM analysis demonstrated that both GO and GO_MPS nanoparticles exhibited low aspect ratio. Conversely, the pristine GO** exhibited the appearance of a "spongy" structure; however, it was observed that post-silanisation the GO nanoparticles lost their porous features and seemed to be covered by coating of silane, showing evidence of nanoparticle aggregation. This loosening of porosity and the formation of agglomerates could have a negative impact in the homogenous dispersion of the nanoparticles and consequently the mechanical performance of the resultant PMMA bone cement.

Although a qualitative understanding of nanoparticle dispersion within PMMA-based bone cement as a function of different silanisation procedures has been achieved. It was difficult to determine nanoparticle dispersion using quantitative methods, which could be a potential limitation of this study. Different measurement techniques (e.g. UV-spectrophotometry and turbidimetry) were investigated, but the data obtained were inconsistent and inconclusive. Additionally, although it is beyond the scope of the current study, it will be essential to assess the potential for cytotoxicity and biocompatibility using appropriate in vitro and in vivo test methods to ensure the nanocomposite bone cement is safe for implantation in the body.

The findings of this work provide an interesting alternative in the preparation of G-PMMA bone cements. The highly notable increase in the dispersion stability of G, and its impact on the mechanical properties suggest that it would be interesting to conduct a more comprehensive study of the potential improvement on the fatigue life and fracture properties. Other aspects, such as the biocompatibility or the effect of the silanisation on the polymerisation process of the PMMA bone cement should be investigated in future works. Finally, the main observations and conclusions outlined in this study could be applied in the future design of silanisation routes for G and GO powders.

5. Conclusions

In this study, we have shown that, to achieve optimised silanisation routes, the features of the G surface oxidation are very significant. The characteristics of the oxygenated groups anchored to the G surface are determinant, because of they are the vehicle by which the silane molecules are anchored to the G. It is postulated that the type of oxygenate group present on the surface (being preferable hydroxyl groups) and the steric hindrance, caused by the presence of high-volume groups, are two important factors to be carefully considered. In addition, a successful method for the silanisation of the G has been developed using 3-methacryloxypropyltrimethoxysilane. The new silanised G demonstrated a marked enhancement in the homogenous dispersion in the nanocomposite cement, which resulted in improved static mechanical properties. Despite the remarkable results obtained with respect to G. The route followed for the silanisation of the GO was not advantageous, which was attributed to the formation of agglomerates and a loss of nanoparticle porosity post-silanisation.

Acknowledgements

The authors would like to thank NanoInnova Technologies, Spain, for supplying the GO powder and to Fernando Pérez (Universidad Pontificia Comillas) for its collaboration.

References

[1] Chen, WF, Hu WM, Li DJ, Chen SN, Dai ZX. A critical review on the development and performance of polymer/graphene nanocomposites. Sci. Eng. Compos. Mater. 25(6): 1059-1073 (2018)

[2] Kulkarni HB, Tambe P, Joshi GM. Influence of covalent and non-covalent modification of graphene on the mechanical, thermal and electrical properties of epoxy/graphene nanocomposites: a review. Compos. Interface. 25(5-7):381-414 (2018).

[3] X. Guan, G. Zheng, K. Dai, C. Liu, X. Yan, C. Shen, Z. Guo. Carbon Nanotubes-Adsorbed Electrospun PA66 Nanofiber Bundles with Improved Conductivity and Robust Flexibility. ACS Appl. Mater. Interfaces. 8, 14150-14159 (2016).

[4] Y. Shi, Z. Chen. Function-driven design of stimuli-responsive polymer composites: recent progress and challenges. J. Mater. Chem. C. Advance Article (2018)

[5] H. Liu, Y. Li, K. Dai, G. Zheng, C. Liu, C. Shen, X. Yan, J. Guob, Z. Guo. Electrically conductive thermoplastic elastomer nanocomposites at ultralow graphene loading levels for strain sensor applications. J. Mater. Chem. C. 4, 157-166 (2016).

[6] Kim, H., Abdala, A.A. & Macosko, C.W. Graphene/Polymer nanocomposites. Macromolecules 43, 6515–6530 (2010).

[7] Wang C, Murugadoss V, Kong J, He ZF, Mai XM, Shao Q, Chen YJ, Guo L, Liu CT, Angaiah S, Guo, ZH. Overview of carbon nanostructures and nanocomposites for electromagnetic wave shielding. Carbon,140:696-733 (2018).

[8] Wang L, Qiu H, Liang CB, Song P, Han YX, Han YX, Gu JW, Kong J, Pan D, Guo ZH. Electromagnetic interference shielding MWCNT-Fe3O4@Ag/epoxy nanocomposites with satisfactory thermal conductivity and high thermal stability. Carbon, 141:506-514 (2018).

[9] Longfei Lv, J Liu, H Liu, C Liu, Y Lu, K Sun, R Fan, N Wang, N Lu, Z Guo, EK Wujcik. An Overview of Electrically Conductive Polymer Nanocomposites toward Electromagnetic Interference Shielding. Eng. Sci. 2:26-42 (2018).

[10] B Kirubasankar, V Murugadoss, J Lin, T Ding, M Dong, L Liu, J Zhang, T Li, N Wang, Z Guo, S Angaian. In-situ grown nickel selenide onto graphene nanohybrid electrodes for high energy density asymmetric supercapacitors, Nanoscale. 10:20414 – 20425 (2018).

[11] Du H, Zhao CX, Lin J, Guo J, Wang B, Hu Z, Shao Q, Pan D, Wujcik EK, Guo Z. Carbon nanomaterials in direct liquid fuel cells, Chemical Record, 18:1365-1372 (2018).

[12] T Su, Q Shao, Z Qin, Z Guo, Z Wu. Role of interfaces in two-dimensional photocatalyst for water splitting, ACS Catalysis, 8:2253-2276 (2018).

[13] Y Zhang, L Qian, W Zhao, X Li, X Huang, X Mai, Z Wang, Q Shao, X Yan, Z Guo. Highly efficient Fe-N-C nanoparticles modified porous graphene composites for oxygen reduction reaction, J. Electrochem. Soc., 165:H510-H516 (2018).

[14] Z Li, B Wang, X Qin, Y Wang, C Liu, Q Shao, N Wang, J Zhang, Z Wang C Shen, Z Guo. Superhydrophobic/superoleophilic polycarbonate/carbon nanotubes porous monolith for selective oil adsorption from water, ACS Sustain. Chem. Eng. 6:13747–13755 (2018).

[15] Y Qian, Y Yuan, H Wang, H Liu, J Zhang, S Shi, Z Guo, N Wang. Highly efficient uranium adsorption by salicylaldoxime/polydopamine graphene oxide nanocomposites, J. Mater. Chem. A, 48, in press (2018).

[16] Tang, L-C., Wan, Y-J., Yan, D., Pei, Y-B., Zhao, L., Li, Y-B., Wu, L-B. The effect of graphene dispersion on the mechanical properties of graphene/epoxy composites. Carbon 60, 16–27 (2013).

[17] Kuila, T., Bose, S., Mishra, A.K., Khanra, P., Kim, N.H., Lee, J.H. Chemical functionalization of graphene and its applications. Prog. Mater. Sci. 57, 1061–1105 (2012).

[18] Ramanathan, T., Stankovich, S., Dikin, D.A., Liu, H., Shen H., Nguyen, S.T., Brinson, L.C. Graphitic nanofillers in PMMA nanocomposites—An investigation of particle size and dispersion and their influence on nanocomposite properties. J. Polym. Sci. Part B Polym. Phys. 45, 2097–2112 (2007).

[19] Kalaitzidou, K., Fukushima, H., Drzal, L.T. Multifunctional polypropylene composites produced by incorporation of exfoliated graphite nanoplatelets. Carbon 45, 1446–1452 (2007).

[20] Kuilla, T., Bhadra, S., Yao, D., Kim, N.H., Bose, S., Lee, J.H. Recent advances in graphene based polymer composites. Prog. Polym. Sci. 35, 1350–1375 (2010).

[21] Y Pan, DW Schubert, JE Ryu, E Wujick, C Liu, C Shen, X Liu. 16. Dynamic Oscillatory Rheological Properties of Polystyrene/Poly(methyl methacrylate) Blends and Their Composites in the Presence of Carbon Black. Eng. Sci., 1:86-94 (2018).

[22] M Dong, Q Li, H Liu, C Liu, E K.Wujcik, Q Shao, T Ding, X Mai, C Shen, Z Guo. Thermoplastic polyurethane-carbon black nanocomposite coating: fabrication and solid particle erosion resistance. Polymer, 158:381-390 (2018).

[23] Gao, C., Liu, T., Shuai, C., Peng, S. Enhancement mechanisms of graphene in nano-58S bioactive glass scaffold: mechanical and biological performance. Sci. Rep. 4, (2014).

[24] Chandrasekaran, S., Sato, N., Tölle, F., Mülhaupt, R., Fiedler, B., Schulte, K. Fracture toughness and failure mechanism of graphene based epoxy composites. Compos. Sci. Technol. 97, 90–99 (2014).

[25] C Wang, M Zhao, J Li, J Yu, S Sun, S Ge, X Guo, F Xie, B Jiang, EK Wujcik, Y Huang, N Wang, Z Guo. Silver nanoparticles/graphene oxide decorated carbon fiber synergistic reinforcement in epoxy-based composites, Polymer, 131:263–271 (2017).

[26] H Gu, H Zhang, C Ma, X Xu, Y Wang, Z Wang, R Wei, H Liu, C Liu, Q Shao, X Mai, Z Guo. Trace electrosprayed nanopolystyrene facilitated dispersion of multiwalled carbon nanotubes: simultaneously strengthening and toughening epoxy, Carbon, 142:131-140 (2019).

[27] Cai, D., Song, M. Recent advance in functionalized graphene/polymer nanocomposites. J. Mater. Chem. 20, 7906 (2010).

[28] Georgakilas, V. Otyepka, M., Bourlinos, A.B., Chandra, V., Kim, N., Kemp, C., Hobza, P., Zboril, R., Kim, K.S. Functionalization of graphene: covalent and non-covalent approaches, derivatives and applications. Chem. Rev. 112, 6156–6214 (2012).

[29] Dunne, N., Clements, J., Wang, J.-S. Acrylic cements for bone fixation in joint replacement. in Joint Replacement Technology (Second Edition) (ed. Revell, P. A.) 212–256 (Woodhead Publishing, 2014).

[30] Chaudhry, S. Dunlop, D. Bone cement in arthroplasty. Orthop. Trauma 26, 391–396 (2012).

[31] Charnley, J. The Classic: The Bonding of Prostheses to Bone by Cement. Clin. Orthop. 468, 3149–3159 (2010).

[32] Sundfeldt, M., V Carlsson, L., B Johansson, C., Thomsen, P., Gretzer, C. Aseptic loosening, not only a question of wear: A review of different theories. Acta Orthop. 77, 177–197 (2006).

[33] Lewis, G. Alternative acrylic bone cement formulations for cemented arthroplasties: Present status, key issues, and future prospects. J. Biomed. Mater. Res. B Appl. Biomater. 84B, 301–319 (2008).

[34] Ormsby, R., McNally, T., Mitchell, C., Dunne, N. Influence of multiwall carbon nanotube functionality and loading on mechanical properties of PMMA/MWCNT bone cements. J. Mater. Sci. Mater. Med. 21, 2287–2292 (2010).

[35] Marrs, B., Andrews, R., Rantell, T., Pienkowski, D. Augmentation of acrylic bone cement with multiwall carbon nanotubes. J. Biomed. Mater. Res. A 77A, 269–276 (2006).

[36] Ormsby, R., McNally, T., Mitchell, C., Dunne, N. Incorporation of multiwalled carbon nanotubes to acrylic based bone cements: Effects on mechanical and thermal properties. J. Mech. Behav. Biomed. Mater. 3, 136–145 (2010).

[37] Paz, E., Forriol, F., del Real, J.C., Dunne, N. Graphene oxide versus graphene for optimisation of PMMA bone cement for orthopaedic applications. Mater. Sci. Eng. C 77, 1003–1011 (2017).

[38] J Zhu, S Wei, J Ryu, M Budhathoki, G Liang, Z Guo. In situ stabilized carbon nanofiber (CNF) reinforced epoxy nanocomposites. J. Mater. Chem., 16:2800-2808 (2006).

[39] J Zhu, S Wei, A Yadav, Z Guo. Rheological behaviors and electrical conductivity of epoxy resin nanocomposites suspended with in-situ stabilized carbon nanofibers. Polymer, 51(12):2643-2651 (2010).

[40] Z Guo, T Pereira, O Choi, Y Wang, HT Hahn. Surface functionalized alumina nanoparticle filled polymeric nanocomposites with enhanced mechanical properties J. Mater. Chem. 20:4937 - 4948 (2010).

[41] Abenojar, J., del Real, J.C., Martinez, M.A., de Santayana, M.C. Effect of silane treatment on SiC particles used as reinforcement in epoxy resins. J. Adhes. 85, 287–301 (2009).

[42] Kim, M.T., Rhee, K.Y., Park, S.J., Hui, D. Effects of silane-modified carbon nanotubes on flexural and fracture behaviors of carbon nanotube-modified epoxy/basalt composites. Compos. Part B Eng. 43, 2298–2302 (2012).

[43] Yang, H., Li, F., Shan, C., Han, D., Zhang, Q., Niu, L., Ivaska, A. Covalent functionalization of chemically converted graphene sheets via silane and its reinforcement. J. Mater. Chem. 19, 4632 (2009).

[44] Jiang, S., Li, Q., Zhao, Y., Wang, J., Kang, M. Effect of surface silanization of carbon fiber on mechanical properties of carbon fiber reinforced polyurethane composites. Compos. Sci. Technol. 110, 87–94 (2015).

[45] Lee, C. Y., Bae, J.-H., Kim, T.-Y., Chang, S.-H., Kim, S. Y. Using silane-functionalized graphene oxides for enhancing the interfacial bonding strength of carbon/epoxy composites. Compos. Part Appl. Sci. Manuf. 75, 11–17 (2015).

[46] Velasco-Santos, C., Martínez-Hernández, A.L., Lozada-Cassou, M., Alvarez-Castillo, A., Castaño, V.M. Chemical functionalization of carbon nanotubes through an organosilane. Nanotechnology 13, 495 (2002).

[47] Avilés, F., Sierra-Chi, C.A., Nistal, A., May-Pat, A., Rubio, F., Rubio, J. Influence of silane concentration on the silanization of multiwall carbon nanotubes. Carbon 57, 520–529 (2013).

[48] Hu, X., Su, E., Zhu, B., Jia, J., Yao, P., Bai, Y. Preparation of silanized graphene/poly(methyl methacrylate) nanocomposites in situ copolymerization and its mechanical properties. Compos. Sci. Technol. 97, 6–11 (2014).

[49] Pantoja M. Martinez MA, Abenojar J, Encinas N, Ballesteros Y. Effect of EtOH/H2O Ratio and pH on Bis-Sulfur Silane Solutions for Electrogalvanized Steel Joints Based on Anaerobic Adhesives. J. Adhesion. 87(7-8):688-708 (2011).

[50] Pantoja M, Abenojar J, Martinez MA. Influence of the type of solvent on the development of superhydrophobicity fromsilane-based solution containing nanoparticles. Appl. Surf. Sci. 397:87-94 (2017).

[51] Pantoja M, Diaz-Benito B, Velasco F, Abenojar J, del Real JC. Analysis of hydrolysis process of gamma-methacryloxypropyltrimethoxysilane and its influence on the formation of silane coatings on 6063 aluminum alloy. Appl. Surf. Sci. 255(12):6386-6390 (2009).

[52] L Xiao, Z Suhe. Measurement of the condensation temperature of nanosilica powder organically modified by a silane coupling agent and its effect evaluation. J. Appl. Polym. Sci. 108(5):3038-3045 (2008).

[53] ISO 5833/2: Implants for surgery. Acrylic resin cements. International Organisation for Standardisation; 2002.

[54] ASTM D 5045: Standard test methods for plane-strain fracture toughness and strain energy release rate of plastic materials. American Society for Testing and Materials. 1999.

[55] Plueddemann, E.P. Chemistry of Silane Coupling Agents. in Silane Coupling Agents (ed. Plueddemann, E. P.) 31–54 (Springer US, 1991). doi:10.1007/978-1-4899-2070-6_2

[56] Guo, Z. Wang, S., Wamg, G., Niu, Z., Yang, J., Wu, W. Effect of oxidation debris on spectroscopic and macroscopic properties of graphene oxide. Carbon 76, 203–211 (2014).

[57] Kim, D.-S., Dhand, V., Rhee, K.-Y., Park, S.-J. Surface treatment and modification of graphene using organosilane and its thermal stability. Arch. Metall. Mater. 60, (2015).

[58] Coates, J. Interpretation if infrared spectra, a practical approach. in Encyclopaedia of Analytical Chemistry (Jhon Wiley & Sons Ltd, 2000).

[59] Avilés, F., Cauich-Rodríguez, J.V., Moo-Tah, L., May-Pat, A., Vargas-Coronado, R. Evaluation of mild acid oxidation treatments for MWCNT functionalization. Carbon 47, 2970–2975 (2009).

[60] Kim, M.T., Rhee, K.Y., Park, S.J.. Hui, D. Effects of silane-modified carbon nanotubes on flexural and fracture behaviors of carbon nanotube-modified epoxy/basalt composites. Compos. Part B Eng. 43, 2298–2302 (2012).

[61] Rourke, J.P., Pandey, P.A., Moore, J.J., Bates, M., Kinloch, I.A., Young, R.J., Wilson, N.R. The Real Graphene Oxide Revealed: Stripping the Oxidative Debris from the Graphene-like Sheets. Agnew. Chem. Int. Ed. 50, 3173–3177 (2011).

[62] Zhi, M., Huang, W., Shi, Q., Ran, K. Improving water dispersibility of non-covalent functionalized reduced graphene oxide with l-tryptophan via cleaning oxidative debris. J. Mater. Sci. Mater. Electron. 27, 7361–7368 (2016).

[63] Velasco-Santos, C., Martínez-Hernández, A.L., Fisher, F.T., Ruoff, R., Castaño, V. M. Improvement of thermal and mechanical properties of carbon nanotube composites through chemical functionalization. Chem. Mater. 15, 4470–4475 (2003).

[64] Kim, D., Dhand, V., Rhee, K., Park, S.-J. Study on the effect of silanization and improvement in the tensile behavior of graphene-chitosan-composite. Polymers 7, 527–551 (2015).

[65] Zhu, Y., Bakis, C.E., Adair, J.H. Effects of carbon nanofiller functionalization and distribution on interlaminar fracture toughness of multi-scale reinforced polymer composites. Carbon 50, 1316–1331 (2012).

[66] Ahmadi-Moghadam, B., Sharafimasooleh, M., Shadlou, S., Taheri, F. Effect of functionalization of graphene nanoplatelets on the mechanical response of graphene/epoxy composites. Mater. Des. 1980-2015 66, 142–149 (2015).

[67] Rafiee, M. A., Rafiee, J., Srivastava, I., Wang, Z., Song, H., Yu, Z.Z., Koratkar, N. Fracture and fatigue in graphene nanocomposites. Small 6, 179–183 (2010).

[68] Marrs, B., Andrews, R., Rantell, T., Pienkowski, D. Augmentation of acrylic bone cement with multiwall carbon nanotubes. J. Biomed. Mater. Res. A 77A, 269–276 (2006).

[69] Ormsby, R., McNally, T., O'Hare, P., Burke, G., Mitchell, C., Dunne, N. Fatigue and biocompatibility properties of a poly(methyl methacrylate) bone cement with multi-walled carbon nanotubes. Acta Biomater. 8, 1201–1212 (2012).

[70] Y. Zhang, M. Zhao, J. Zhang, Q. Shao, J. Li, H. Li, B. Lin, M. Yu1, S. Chen, Z. Guo. Excellent corrosion protection performance of epoxy composite coatings filled with silane functionalized silicon nitride. J. Polym. Res. 2018, 25, 130.

[71] Ma, P. C., Kim, J.-K., Tang, B. Z. Functionalization of carbon nanotubes using a silane coupling agent. Carbon 44, 3232–3238 (2006).

[72] Kathi, J., Rhee, K. Y. Surface modification of multi-walled carbon nanotubes using 3-aminopropyltriethoxysilane. J. Mater. Sci. 43, 33–37 (2008).

[73] Iimura, K., Nakajima, Y., Kato, T. A study on structures and formation mechanisms of self-assembled monolayers of n-alkyltrichlorosilanes using infrared spectroscopy and atomic force microscopy. Thin Solid Films 379, 230–239 (2000).

[74] Krasnoslobodtsev, A. V. & Smirnov, S. N. Effect of Water on silanization of silica by trimethoxysilanes. Langmuir 18, 3181–3184 (2002).

[75] Gutowski, W.S., Wu, D.Y. & Li, S. Surface silanization of polyethylene for enhanced adhesion. J. Adhes. 43, 139–155 (1993).

[76] Xu, D. et al. Hydrolysis and silanization of the hydrosilicon surface of freshly prepared porous silicon by an amine catalytic reaction. New J. Chem. 27, 300–306 (2003).

[77] Packham, D.E. Handbook of adhesion. 2nd Edition. John Wiley (2005).

[78] Plueddemann, E. P. Silane coupling agents. Springer (1991).

[79] Mittal, K.L. Silanes and other coupling agents, volume 5: [proceedings of the Sixth International Symposium on Silanes and Other Coupling Agents held at the University of Cincinnati, Cincinnati, OH, June 13 - 15, 2007 under the auspices of MST Conferences]. (VSP, 2009).

[80] Yang, J., Shi, G., Tu, Y., Fang, H. High Correlation between Oxidation Loci on Graphene Oxide. Agnew. Chem. Int. Ed. 53, 10190–10194 (2014).

[81] Thomas, H. R., Phillips, D. J., Wilson, N. R., Gibson, M. I., Rourke, J. P. One-step grafting of polymers to graphene oxide. Polym Chem 6, 8270–8274 (2015)